Exp Brain Res (1999) 124:118–136

RESEARCH ARTICLE

Dagmar Sternad · Stefan Schaal

Segmentation of endpoint trajectories does not imply segmented control

Received: 20 March 1998 / Accepted: 14 July 1998

Abstract While it is generally assumed that complex movements consist of a sequence of simpler units, the quest to define these units of action, or movement primitives, remains an open question. In this context, two hypotheses of movement segmentation of endpoint trajectories in three-dimensional human drawing movements are reexamined: (1) the stroke-based segmentation hypothesis based on the results that the proportionality coefficient of the two-thirds power law changes discontinuously with each new "stroke," and (2) the segmentation hypothesis inferred from the observation of piecewise planar endpoint trajectories of three-dimensional drawing movements. In two experiments human subjects performed a set of elliptical and figure eight patterns of different sizes and orientations using their whole arm in three dimensions. The kinematic characteristics of the endpoint trajectories and the seven joint angles of the arm were analyzed. While the endpoint trajectories produced similar segmentation features to those reported in the literature, analyses of the joint angles show no obvious segmentation but rather continuous oscillatory patterns. By approximating the joint angle data of human subjects with sinusoidal trajectories, and by implementing this model on a 7-degree-of-freedom (DOF) anthropomorphic robot arm, it is shown that such a continuous movement strategy can produce exactly the same features as observed by the above segmentation hypotheses. The origin of this apparent segmentation of endpoint trajectories is traced back to the nonlinear transformations of the forward kinematics of human arms. The presented results demonstrate that principles of discrete movement generation may not be reconciled with those of rhythmic movement as easily as has been previously suggested, while the generalization of nonlinear pattern generators to arm movements can offer an interesting alternative to approach the question of units of action.

Key words Human arm movements · Coordination · Segmentation · Piecewise planarity · Power law

D. Sternad (✉)
Department of Kinesiology, Pennsylvania State University, 266 Recreation Building, University Park, PA 16802, USA
e-mail: dxs48@psu.edu
http://www.psu.edu/personal/faculty/d/x/dxs48

S. Schaal (✉)
Computer Science and Neuroscience, HNB-103, University of Southern California, Los Angeles, CA 90089-2520, USA
sschaal@usc.edu, http://www-slab.usc.edu/sschaal

D. Sternad · S. Schaal
Kawato Dynamic Brain Project (ERATO/JST), 2-2 Hikaridai, Seika-cho, Soraku-gun, 619-02 Kyoto, Japan

Introduction

Given the continuous stream of movements that biological systems exhibit in their daily activities, an account of such versatility has typically assumed that there are movement segments that are concatenated together. Therefore, a fundamental question that has pervaded research in motor control revolves around defining such units of action. Typical examples of movements where units seem to be strung together into a meaningful sequence are handwriting, typing, and speech production and, to a large degree, it is these types of tasks that have motivated the search for units of action. Evidently, the definition of an elementary unit crucially depends on the task, but, given the level of analysis and, in relation, the choice of a reference system in which actions are assumed to be generated, general propositions have been made.

Historically, the first contributions to this discussion originated in neurophysiological research. Since Sherrington's (1906) seminal work, the spinal reflex has been viewed as the irreducible building block which is embedded in more complex functional behavior. To utilize the concept of the reflex as a primitive for longer behavioral sequences, the ensuing behaviorist school of thought proposed the chaining of stimulus-response units by association (see review in Lashley 1951). While this account was soon discarded as too simplistic, the nesting of reflexes into a functional hierarchy or heterarchy has subsequently been suggested as a more adaptive exten-

sion (e.g., Easton 1972). Spinal reflexes also played an important role in the development of different variants of the equilibrium point hypothesis, from Merton's early proposition to later formulations of the α- or λ-model (Bizzi et al. 1984; Bizzi et al. 1976; Feldman 1966; Latash 1993; Mertens 1953). While this line of research has in the main focused on discrete tasks, there have also been suggestions to generalize the equilibrium point concept to rhythmic movements in terms of an alternating sequence of discrete equilibrium point shifts (Adamovich et al. 1994; Feldman 1980; Latash 1993). Another influential result from physiological research was that endogenous neural circuits at the spinal level, i.e., rhythmic movement primitives, can produce complex movement patterns, specifically rhythmic locomotory activity (Brown 1914; Cohen 1992; Grillner 1975). Instead of assuming discrete segments that need to be strung together, primacy is given to rhythmic units as versatile building blocks in generating complex action patterns, called central or motor pattern generators (CPGs or MPGs). Although CPGs could be identified as oscillatory units of action in a number of species, the concept still awaits successful generalization to complex behavior of higher vertebrates.

While at the neurophysiological level of inquiry the components of action are sought in the underlying neural substrate, research in psychology has typically chosen the level of task or behavior as its primary entry into identifying units of action. At this more macroscopic level of investigation, the idea of CPGs as rhythmic units of action has found a parallel in the dynamic systems perspective to movement coordination. This approach proposes oscillatory regimes to give expression to the stable rhythmic patterns arising within a task; again interlimb coordination typifying locomotion was the primary focus (Haken et al. 1985; Kay et al. 1987; Kelso 1994; Sternad et al. 1996). In contrast to CPGs, these autonomous oscillatory regimes are not assumed to map directly onto neural structures, but rather to emerge on a functionally defined task level. Similar to how the concept of discrete units of action was extended to account for rhythmic movements, the concept of oscillators was also explored to account for discrete reaching tasks (Schöner 1990, 1994) and for serial aspects of movements (Sternad, Saltzman, and Turvey, 1998).

Since the 1980s, another entry into the problem of identifying movement segments has become prominent, emphasizing movement trajectories and the analysis of their kinematic features. In particular, a series of studies examined the characteristics of endpoint trajectories of arm movements with the objective of determining the reference system in which movement trajectories are planned. By recording arm trajectories in point-to-point planar reaching movements, Morasso (1981) concluded from the straightness of endeffector trajectories that movements are planned in extrinsic space as opposed to joint angular or muscle coordinates. In a subsequent study, Morasso (1983) extended his finding by reporting that also three-dimensional trajectories of the endpoint of an arm consisted of segments that were piecewise planar. He rested this conclusion on analyses that showed that curvature and angular velocity of the three-dimensional trajectory were systematically related in piecewise planar units. While these results speak to segmentation into linear or planar strokes of the endpoint trajectory (see also Abend et al. 1982; Flash and Hogan 1985), the fact that linearity of the endpoint trajectory is an unequivocal sign for extrinsic planning was questioned by Hollerbach and Atkeson (1987). These authors demonstrated that, with the exception of trajectories involving joint reversals, two-dimensional linear trajectories can similarly be produced by straight joint-space trajectories when the onsets of the joint angle displacements are staggered in time. Similarly, Uno et al. (1989) showed in their minimum-torque change model that trajectories planned in joint coordinates can reproduce the linear trajectories observed in human data. These studies highlight that the kinematics of the endpoint trajectory alone cannot provide sufficient evidence for either intrinsic or extrinsic planning.

The present investigation will demonstrate that, for three-dimensional movements, an apparent segmentation of endpoint trajectories does not warrant the inference of a segmented control strategy. Instead, a continuous control signal at the level of joint space can produce a seemingly segmented trajectory of the endpoint trajectory. In particular, it is our goal to reinvestigate two propositions in the literature on movement segmentation in human arm movements.

Segmentation based on the two-thirds power law

Studying handwriting and two-dimensional drawing movements, Viviani and Terzuolo (1980) first identified a systematic relationship between angular velocity and curvature of the endeffector traces, an observation that was subsequently formalized in the "two-thirds power law" (Lacquaniti et al. 1983):

$$a(t)=k\,c(t)^{2/3} \tag{1}$$

where $a(t)$ denotes the angular velocity of the endpoint trajectory and $c(t)$ the corresponding curvature; this relation can be equivalently expressed by a one-third power-law relating tangential velocity $v(t)$ to radius of curvature $r(t)$:

$$v(t)=k\,r(t)^{1/3} \tag{2}$$

Since there is no physical necessity for movement systems to satisfy this relation between kinematic and geometric properties, and since the relation has been reproduced in numerous experiments (for an overview see Viviani and Flash 1995), the two-thirds power law has been interpreted as an expression of a fundamental constraint of the CNS, although biomechanical properties may significantly contribute (Gribble and Ostry 1996). Additionally, Viviani and Cenzato (1985) and Viviani (1986) investigated the role of the proportionality con-

stant k as a means to reveal movement segmentation: as k is approximately constant during extended parts of the movement and only shifts abruptly at certain points of the trajectory, it was interpreted as an indicator for segmented control. Since the magnitude of k also appears to correlate with the average movement velocity in a movement segment, k was termed the "velocity gain factor." Viviani and Cenzato (1985) found that planar elliptical drawing patterns are characterized by a single k and, therefore, consist of one unit of action. However, in a fine-grained analysis of elliptic patterns of different eccentricities, Wann et al. (1988) demonstrated consistent deviations from this result. Such departures were detected from an increasing variability in the log v log r regressions for estimating k and the exponent β of Eq. 2, and ascribed to several movement segments each of which having a different velocity gain factor k.

Segmentation based on piecewise planarity

The second segmentation hypothesis we want to address partially arose from research on the power law. Soechting and Terzuolo (1987a,b) provided qualitative demonstrations that three-dimensional rhythmic endpoint trajectories are piecewise planar. Using a curvature criterion as the basis for segmentation, they confirmed and extended Morasso's (1983) results that rhythmic movements are segmented into piecewise planar strokes. After Pellizzer et al. (1992) demonstrated piecewise planarity even in an isometric task, movement segmentation into piecewise planar strokes has largely been accepted as one of the features of human and primate arm control.

Goals and research strategy

The main assumption underlying these two segmentation hypotheses is that observed features of the endpoint trajectory give direct evidence for principles inherent in movement generation. In this study, it will be argued that such an assumption potentially overlooks the contributions of the kinematic properties of the arm which may be responsible for the above features. In order to make this point, our experiments will investigate two movement patterns that were examined repeatedly in the literature (ellipses and figure eights); however, we will introduce novel variations in size, shape and orientation. These experimental conditions will allow us to determine the influence of nonlinear transformations that the forward kinematics of a 7-degree-of-freedom (DOF) arm adds to the realization of endpoint trajectories. In the literature, these influences were only marginally significant as these studies typically investigated relatively small drawing patterns where the forward kinematics is approximately linear. For the rhythmic drawing patterns employed in our experiments, we will demonstrate that:

1. Endpoint trajectories in rhythmic arm movements can be approximated by continuous oscillatory movements at the level of the biomechanical degrees of freedom of the arm. These results confirm previous data of Soechting and Terzuolo (1986) and Soechting et al. (1986) and also relate to the work of Hollerbach (1981).
2. The segmentation of the endeffector trajectory inferred from abrupt changes of the velocity gain factor can be a product of the geometry of the effector system and does not warrant the unequivocal conclusion of segmented control.
3. Piecewise planar segmentation of the endeffector trajectory arises even in continuous oscillatory control as a by-product of the nonlinear kinematics transformation that maps the joint angle trajectories into endpoint trajectories, and is therefore not necessarily a sign of segmented planning units.

To present these arguments, the study adopts the following strategy. First, in two experiments, human subjects perform cyclic drawing movements in three dimensions. Importantly, subjects use their whole arm and the patterns are scaled in size, shape and orientation to examine the influence of the kinematics of the arm on the endpoint trajectory. Data are recorded from the endpoint and seven joint angles. Second, the joint angular trajectories are approximated by continuous sine waves. Third, based on these sinusoidal fits, the human joint movements are implemented and executed on a 7-DOF anthropomorphic robot arm. Fourth, the hand paths of the robot resulting from this continuous control strategy are recorded in the same way as in the human experiments and are compared to those of the subjects. Fifth, phenomena of the real data are explained in simulations with a simplified arm, demonstrating that the observed "indicators for segmentation" can be accounted for by the nonlinear transformations of the arm's kinematic chain.

This methodology allows the direct comparison of data from human subjects with data from an artificial system whose control strategy is known. Using a robot instead of a simulation enables us to measure the artificial data with exactly the same devices as the human data, such that both data sets undergo the same distortions from data recording and data processing. In addition, the stringent constraints of an implementation on an actual robot helped assure the correctness of our statements and their applicability to a real anthropomorphic movement system.

Materials and methods

Participants

Five volunteers from our laboratory (two female, three male) participated in the experiment. Their ages ranged between 24 and 38 years. All of them were right-handed and did not report any previous arm injuries. The experiments had been approved by the ethics committee and subjects gave their informed consent prior to their inclusion in the study.

Fig. 1 The experimental setup

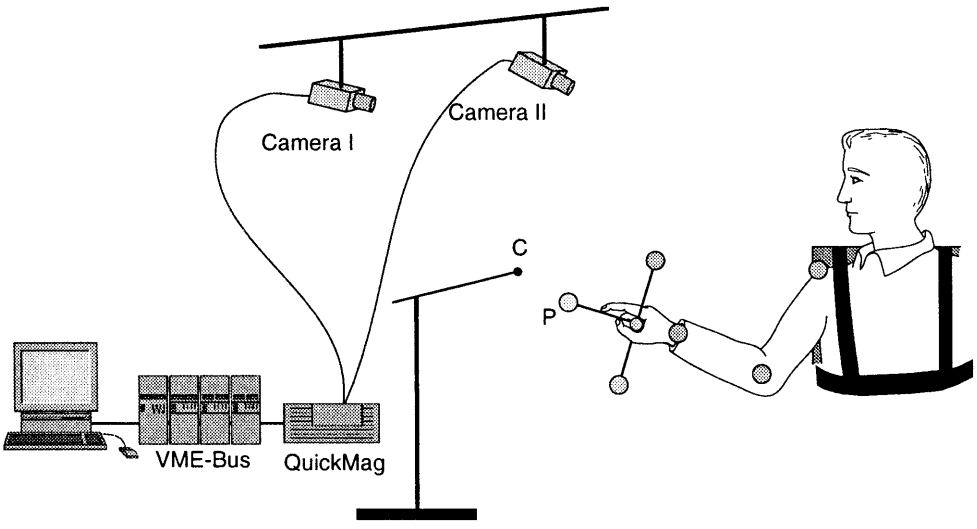

Data Recording

Subjects were seated in a dentist's chair with a high rigid back rest and their shoulder and waist was strapped to the chair with adjustable seatbelts to avoid movements of the shoulder, particularly of the sternoclavicular and acromioclavicular joints and the scapula. Prior to data collection, three colored spherical markers (diameter 0.03 m) were attached with adhesive material to the skin over the bony parts of the shoulder, elbow and wrist joints. Three additional markers were attached to the ends of a hand-held, lightweight aluminum "cross" with rod lengths of 0.15 m measured from the cross point (Fig. 1). The marker denoted as "P" served as the "pointer," or working point, with which subjects drew the required figures in the experiments. The trajectories of the centroids of the six markers were recorded in three Cartesian dimensions with a color vision-based motion analysis system (QuickMag, Japan). The QuickMag system can track six markers simultaneously as long as their colors are sufficiently different. Data were collected at 60 Hz and stored in a Motorola MVME68040 CPU, mounted in a VME bus, running the real-time operating system VxWorks. For long-term storage and further analysis, the data were transferred and postprocessed on a SunSparc workstation.

Robot

Figure 2 depicts the anthropomorphic robot arm that was used in the reported experiments (Sarcos Dexterous Arm, Salt Lake City, UT, USA). The arm has 7 DOF in a configuration that mimics a human arm with a 3-DOF shoulder joint, a 1-DOF elbow, and a 3-DOF wrist joint (the finger joints can be neglected for present purposes). The design of the arm was inspired by biomechanical studies of human arms (Wood et al. 1989). Except for shoulder flexion-extension, the degrees of freedom of the arm are approximately identical to those of the human arm (see Fig. 3). To allow a direct comparison between the joints of the robot arm and the measured human joint data, the difference in the geometrical arrangement of the SFE joint was corrected for by a coordinate transformation (for details see Craig 1986). For control, the robot employs kinematic trajectory plans (joint position, velocity, and acceleration), converts these to joint torques by an inverse dynamics model based on estimated parameters (An et al. 1988), and executes the torque commands in conjunction with a low-gain PID controller. Position and velocity feedback is generated from high-resolution optical encoders and incorporated into the digital servo-loop. The torque commands are executed by hydraulic motors in each degree of freedom which, in a low-level analog loop, servo-regulate about a given torque value by means of torque sensors in each joint. Eight parallel processors in a VME bus generate the appropriate feedforward and feedback torque commands (sampling frequency: 480 Hz). The lengths of the arm segments correspond to those of a tall human being with a total arm length of 0.94 m (shoulder to finger tip). The total weight of the arm is 24 kg. The hydraulic motors are powered by a 207-bar pump. A more detailed description of the robot can be found in Korane (1991). Despite the size and weight difference between the robot and a human arm, the feedforward/feedback control strategy produced excellent agreement between the planned and the executed trajectories of the robot.

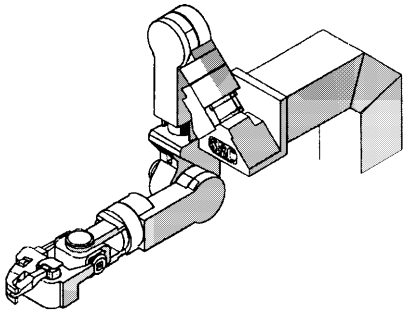

Fig. 2 The Sarcos dexterous arm

Procedure

Trials with elliptical patterns

After the participant was seated, they were instructed to draw a series of ellipses with their dominant arm in the horizontal plane. The experimental patterns were comparable to the ones used in previous work (Viviani and Schneider 1991; Soechting and Terzuolo 1986; Soechting et al. 1986). The experimenter demonstrated the elliptic patterns and their approximate orientation with respect to the body. No extrinsic constraints were given that would confine the ellipse to a plane. The first set of ellipses was drawn so that the long axis of the ellipse was roughly parallel to the *x*-axis (Fig. 3). A second set of ellipses was drawn in a diagonal orientation with the long axis pointing approximately from the center of the chest 45° to the right in the *x*–*y* plane. This diagonal orientation was chosen because joint limits are not so easily encountered as in other orientations (Viviani and Schneider 1991). The experimental trials were performed in two blocks, each consisting of ten trials. In one block all the elliptic patterns were performed in the same orientation and with approximately the same eccentricity,

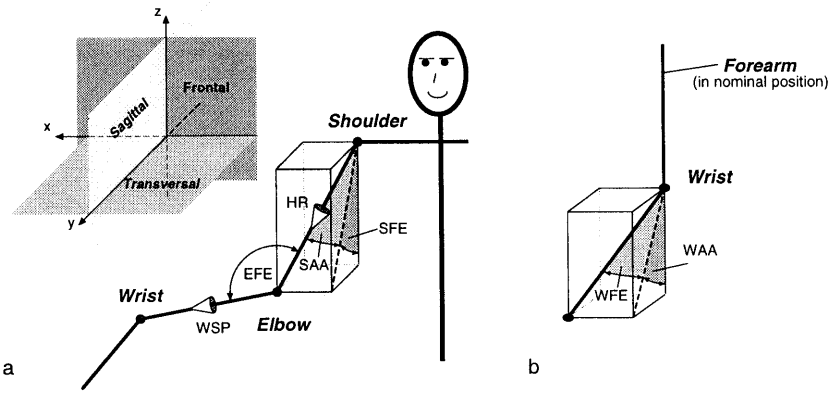

Fig. 3 a The coordinate system used for joint angles: shoulder flexion-extension (*SFE*) is the angle between the *z*-axis and the projection of the upper arm onto the sagittal plane; shoulder adduction-abduction (*SAA*) is the angle between the upper arm and the projection of the upper arm onto the sagittal plane; humeral rotation (*HR*) is the torsion angle about the upper arm; elbow flexion-extension (*EFE*) is the angle between upper and forearm in the plane spanned by the two limb segments; wrist supination-pronation (*WSP*) is the torsion angle about the forearm. **b** The wrist angles are defined relative to a nominal posture of the forearm and hand: the nominal posture is the forearm hanging straight down while the palm is parallel to the sagittal plane and facing towards the body. Wrist flexion-extension (*WFE*) is the angle enclosed between the hand and the projection of the hand onto the sagittal plane; wrist adduction-abduction (*WAA*) is the angle between the *z*-axis and the projection of the hand onto the sagittal plane

but at approximately five different sizes. Prior to the actual data collection, participants were asked to explore their workspace and practice different sizes of ellipses with the only constraint being that for the largest patterns they should avoid getting into extreme ranges of motion. The first trial of each block started with an intermediate-sized ellipse followed by ellipses in the following sequence of sizes (1 denotes the smallest, 5 denotes the largest ellipse, and 3 is the intermediate size): 3-4-5-3-2-1-5-4-1-2. This staggered order was chosen because participants could and should not remember the absolute sizes of the ellipses. By going through different sizes in this step-like fashion all subjects could produce a roughly uniform distribution of different-sized ellipses between a maximal and minimal size. It was emphasized that throughout one trial the patterns should be consistent in size. For the actual data collection, subjects started the pattern, then they closed their eyes to avoid visual orientation in Cartesian coordinates and, while continuing the pattern, they verbally signaled to the experimenter when they were ready for data recording. The order of the two blocks was counterbalanced across subjects. Data collection lasted for 15 s. Participants could rest their arms between trials whenever they needed. The total experiment lasted approximately 25 min.

Trials with figure eight patterns

In the second experiment, participants were instructed to draw a series of figure eight patterns in the frontoparallel plane with the pointer in their dominant hand, as described by Soechting and Terzuolo (1987a,b). A rod mounted on a tripod provided an initial orientation point, marked “C” in Fig. 1, that indicated the center of the pattern. The marker was individually adjusted so that for each subject the figure eight was centered approximately at shoulder height. The marker was far enough away that it did not interfere with the movement. The first series of patterns consisted of ten trials with figure eights in standing orientation of different width/height ratios, again with the goal to uniformly cover a range of pattern sizes between a maximal and minimal size. The height of the pattern was approximately between 0.5 and 0.7 m, while the width of the figure eight was varied systematically. The variations started with a figure eight of zero width, i.e., it was “degenerated” to a line. The width was increased in four steps with the goal of systematically increasing the width/height ratio of the figure eight approximately to one (height is measured as the total height across two lobes), corresponding to a “squashed” figure eight. After one repetition of the largest pattern the size was decreased in four steps back to zero width. The gradations were chosen by the participant and no visual templates were given. Again, it was emphasized that the patterns should be consistent throughout one trial while the actual size and location in space was only a secondary requirement. Subjects practiced different width/height ratios of figure eights prior to the actual data collection to acquaint themselves with their workspaces. They were asked to stay away from the extreme ranges of motion of the arm joints. For the actual data collection, subjects started a pattern with their eyes open in order to scale the pattern appropriately and center it around “C”. While continuing the pattern, they closed their eyes and verbally signaled to the experimenter when they were ready for data collection. One trial lasted for 15 s. Participants could rest their arms between trials whenever they needed. The same experimental procedure was repeated for lying figure eights in the frontoparallel plane.

Data analysis

Data filtering

The three-dimensional trajectory of each marker was checked for missing data samples using a status number provided by the QuickMag system. Missing data points, for instance due to short occlusions, were linearly interpolated from the nearest valid data points. All trajectories were low-pass filtered with a zero-lag second-order Butterworth filter with 4.5-Hz cutoff frequency. For the analysis of the endpoint trajectory, the marker “P” was additionally high-pass filtered with a second-order zero-lag Butterworth filter (cutoff frequency 0.3 Hz). This filter eliminated slow drifts of the drawing pattern in space due to the blindfolded pattern execution. After filtering, the first and last 60 data points of each trial were discarded to eliminate distortions from digital filter onsets. Smooth differentiable trajectories of each marker were obtained by a minimum jerk spline approximation, adapted from Wada and Kawato (1994). This spline method has the advantage that derivatives up to order five of the trajectories can be obtained analytically by differentiating the spline equations, while the spline approximation itself does not require the computation of numerical derivatives. The reconstructed trajectories were guaranteed to lie within 0.01 m Euclidean distance from the measured trajectory. On average, they were within 0.001–0.002 m distance of the measured trajectory.

Joint angle reconstruction

The six measured markers allowed an analytically well defined reconstruction of the joint trajectories of the subjects. We used a def-

inition of the joint coordinates that is related to the biomechanical degrees of freedom of the human arm, as suggested by Wood et al. (1989). Figure 3 illustrates this coordinate system. The seven joint angles are obtained by recursive kinematics calculations starting from the shoulder and working down to the wrist with the goal of transforming the arm into a nominal arm posture. The nominal posture was defined as the one where the entire arm hangs straight down with the palm parallel to the sagittal plane and facing towards the body. The reconstructed joint angles were checked against outlying data and other possible errors by comparing the results of two three-dimensional graphic simulations performed for each experimental trial of each subject: one simulation used the time series of the three-dimensional markers as recorded by the motion tracker to animate a stick figure arm by connecting the three-dimensional markers appropriately. The second simulation used the time series of the reconstructed joint angles to animate the same stick figure by using the forward kinematics of the arm. Both movement simulations were compared visually and numerically and were in exact agreement.

Based on the finding that cyclic drawing patterns are produced by approximately sinusoidal oscillations in joint space (see Soechting et al. 1986; Soechting and Terzuolo 1986), the seven joint angle trajectories were fitted with sinusoids. The fundamental frequency of each pattern was determined as the average of the fundamental peaks of FFT analyses of each of the seven joint angle trajectories. This method is reliable as the patterns were performed stably over the 15-s trials. The standard deviations around the mean fundamental were in the order of approximately 0.2 Hz. The averaging was needed to eliminate the discretization errors that a FFT introduces on discrete data. Given the fundamental frequency, the amplitudes and phases of sinusoidal fits of the joint trajectories were approximated by the Levenberg-Marquardt nonlinear regression (Press et al. 1989). As a result, a complete approximation of each trial was obtained in terms of sinusoidal joint motion, together with a coefficient of determination indicating the quality of fit of each sinusoid.

In order to fit the figure eight patterns with sinusoids, the above procedure needed to be modified in the following fashion: first, the fundamental frequency of each pattern was determined from the fundamental peak of the FFT analyses averaged over the seven joint angle trajectories, as for the elliptic trajectories – again, the FFT peaks coincided sufficiently well such that the subsequent averaging resulted in reliable mean values with low standard deviation. Second, as figure eight patterns require that some joint angles move at twice the fundamental frequency, all power spectra of all joints were examined for a second peak. This procedure resulted in two candidate frequencies for each joint, either at period one or period two. The frequency with the largest FFT power was chosen to be the characteristic frequency of the degrees of freedom. As the joint trajectories, especially of "slim" figure eight patterns, were sometimes contaminated by peaks resulting from interaction torques, it could occur that the characteristic frequency of a joint angle was determined incorrectly. Such errors were corrected by enforcing that across all trials of one pattern orientation, each joint angle was consistently either period one or period two. Whether period one or period two was chosen was decided based on which frequency occurred most often across trials.

Descriptive measures of the endpoint trajectory

Perimeter. The mean perimeter of each pattern was obtained by summing over the Euclidean distances of subsequent data points and dividing by the number of elliptical or figure eight cycles per trial. The number of repeated cycles was obtained from the fundamental frequency of the FFT analysis of each pattern and the trial duration.

Width/height ratio. An estimate of the width/height ratio of the elliptical and the figure eight patterns was obtained from the covariance matrix of all data points per trial. The eigenvalues of the covariance matrix were used as indicators of the spatial extension of the pattern. The square root of the ratio of the second largest and the largest eigenvalue indicated the width/height ratio. In the special case of zero width of the figure eight patterns, the ratio had to be computed from the ratio of the smallest to the largest eigenvalue.

Planarity. Elliptical patterns were first split into trajectory pieces of one period duration. Planarity of the elliptical patterns was estimated by determining the square root of the smallest eigenvalue[1] of the covariance matrix of each trajectory piece, and then by averaging over these values. Planarity for the figure eight patterns was calculated by first determining the node of each figure eight and splitting the entire trial into trajectory pieces separated by the node. Subsequently, planarity was calculated for all individual trajectory pieces as described for the ellipses. Finally, the planarity estimate for a complete figure eight trial was calculated as the average planarity of all trajectory pieces. For the degenerated figure eight, the "node" was determined as the median of the curvilinear pattern. Given this point, planarity was calculated as for normal figure eights, except that planarity of the trajectory pieces was obtained as the square root of the second largest eigenvalues of the covariance matrix. Performing the calculations on a cycle-by-cycle basis was necessary to avoid noise effects from slow drifts in the subjects' performance.

Angle between figure eight lobes. The calculation of the planarity of the figure eights simultaneously yields the normal vector of the approximated plane in which a trajectory piece lies: the normal vector is the eigenvector corresponding to the smallest eigenvalue of the covariance matrix of a trajectory piece. By averaging over all normal vectors belonging to individual trajectory pieces of one figure eight lobe, the mean normal of each of the two lobes was obtained. The angle between the figure eight lobes was the angle between the two mean normal vectors. For degenerate figure eight, appropriate corrections of the calculations were made in analogy to calculating planarity.

Power law exponent. The radius of curvature and the tangential velocity of the elliptical patterns were calculated according to standard formulae (e.g., Morasso 1983). The velocity gain factor k and the exponent β of the power law were estimated using the Levenberg-Marquardt nonlinear least-squares regression (Press et al. 1989). This regression also provided a coefficient of determination which served as a measure for the quality of fit of the power law relation.

---

[1] Although the smallest eigenvalue is generally very vulnerable to noise, the calculated values from the present data set nevertheless provide a reliable indicator for planarity: We assume that the collected data were generated by a deterministic movement system that has (a) additive noise which is identical in all measured variables due to the data recording device and (b) a slow drift (i.e., significantly slower than the period). If the data were perfectly planar, the smallest eigenvalue of the covariance matrix of the data corresponds to the variance of the noise. Our measure of planarity is thus lower bounded by the noise in the data after filtering. Therefore, an increase in this planarity measure with pattern size can only be due to a decreasing planarity of the data, or an increase in drift of the pattern (the recording noise is constant). Since the focus of the analysis is on the change of this measure across pattern size, the constant offset due to noise is of minor concern. To exclude that the slow drift can significantly contaminate the data, the eigenvalues were computed period by period. Due to the "isochrony" (Viviani and Terzuolo 1982) that we observed in our data, approximately the same number of data points entered into the eigenvalue calculations for patterns of different size, within one pattern orientation and subject. Therefore, possible contaminations of the planarity measure due to a change of sample size for the eigenvalues determination were minimal.

Table 1 Kinematic measures of the five subjects performing the two extreme sizes of the ten elliptic patterns drawn in frontal and oblique orientation, respectively

	Frontal orientation				Oblique orientation			
	Perimeter (m)		Planarity (m)		Perimeter (m)		Planarity (m)	
	Small	Large	Small	Large	Small	Large	Small	Large
Subject 1	0.374	1.764	0.004	0.019	0.241	0.921	0.004	0.012
Subject 2	0.504	1.759	0.005	0.020	0.362	1.248	0.004	0.013
Subject 3	0.197	1.341	0.004	0.024	0.272	0.928	0.007	0.014
Subject 4	0.514	1.456	0.003	0.009	0.405	1.195	0.005	0.008
Subject 5	0.270	1.807	0.004	0.012	0.184	1.178	0.004	0.011

Data modeling and robot implementation

In order to replicate the human data with the anthropomorphic robot, the ten trials of each subject from one set of different-sized patterns were sorted according to their mean perimeters. For each joint angle a weighted regression analysis (Myers 1990) was performed regressing each of the three parameters of the sinusoid (frequency, amplitude, phase) against the perimeter. Weighting the regression analyses was necessary since the parameters of the sinusoidal fits for the different-sized joint trajectories had different variances. A nonweighted regression over such data would violate the linear regression model which assumes equal variance in all data points. Since the true variance of the sinusoidal fit parameters is not easily obtained in a nonlinear regression, we used the coefficient of determination of the sinusoidal fit as a weight, assuming that it approximately reflects the reciprocal of the variance of the coefficients of the sinusoidal fits. Thus, the weighted regression deemphasized the influence of data points stemming from sinusoidal fits with low coefficients of determination.

As the final result of the regressions, we obtained linear scaling relations of how the joint angle motions varied as a function of the pattern size in terms of frequency, amplitude, and phasing. From these scaling relations, we generated the desired joint positions, velocities, and accelerations for five pattern sizes, starting at the smallest perimeter and increasing in constant steps until the largest perimeter was reached. This description of joint motion sufficed to repeat the patterns with the anthropomorphic robot arm. We recorded the Cartesian finger-tip movement – corresponding to marker "P" of the human subjects – of the robot with the QuickMag vision system for 15 s for each movement pattern. For comparison, we also stored the desired and the actual finger-tip movement of the robot as available from forward kinematics computations based on the planned and actual joint motion; the actual joint motion was available through high-resolution optical encoders in the robot joints. Thus, the pattern realized by the robot could be analyzed in the same way as the human data. Additionally, we obtained calibration information about the quality of the data processing of the vision-based motion analysis by comparing the visual data with much higher precision data from the internal sensors of the robot.

Results

Elliptical patterns

Descriptive measures of the endpoint trajectories

The descriptive kinematic measures of the frontal and the oblique ellipses for each of the five subjects are summarized in Table 1, listing the perimeter and planarity measure for the smallest and the largest ellipses of the ten trials. In all subjects the perimeters increase approximately 3–6 times from the smallest to the largest pattern. The measure of planarity corresponds to the standard deviation of the data orthogonal to the major principal components. Therefore, the generally small numbers indicate that the elliptic trajectories lie approximately in a plane. However, the values for planarity increase with the perimeter, demonstrating that larger patterns systematically deviate from a two-dimensional extension. Note that subjects closed their eyes in order to avoid orientation of the ellipses to any external planar reference, like a wall in the laboratory, such that their movements reflected as closely as possible their inherent movement strategy. The values of the eight intermediate-sized ellipses, not listed in the table, scaled up approximately evenly within the range shown in the table. Figure 4a,b shows representative examples of elliptic trials of one subject in both pattern orientations.

Power law and velocity gain factor

The endpoint trajectories of human data were used to determine the coefficients of the power law. Table 2 summarizes the fitted exponents β of the power law together with the R^2 values of the regression. While β of the small ellipses in both orientations is close to the predicted value 1/3 (we used the second formula in Eq. 2 to obtain the power law fits), β deviates more for the larger ellipses (see also Wann et al. 1988). Important for the argument below is that the R^2 values decrease significantly from the small to the large ellipses, in both the frontal and the oblique orientation (frontal: $t(4)=4.2$; $P<0.01$; oblique: $t(4)=6.7$; $P<0.002$).

Following Lacquaniti et al. (1983), a useful method to inspect the power law fit is to plot tangential velocity v against the radius of curvature r raised to the power 1/3 (referred to as v–r plot from now on). If the power law holds, the data lie on a straight line through the origin with the slope expressing the velocity gain factor k. During one elliptic cycle the continuous trajectory traverses the same linear slope 4 times. Importantly, if the data lie on more than one line throughout one elliptic cycle, this has been interpreted as evidence for different segments (Viviani 1986; Viviani and Cenzato 1985). Figure 5a shows the v–r plots for three sizes of ellipses taken from one representative subject. For the small el-

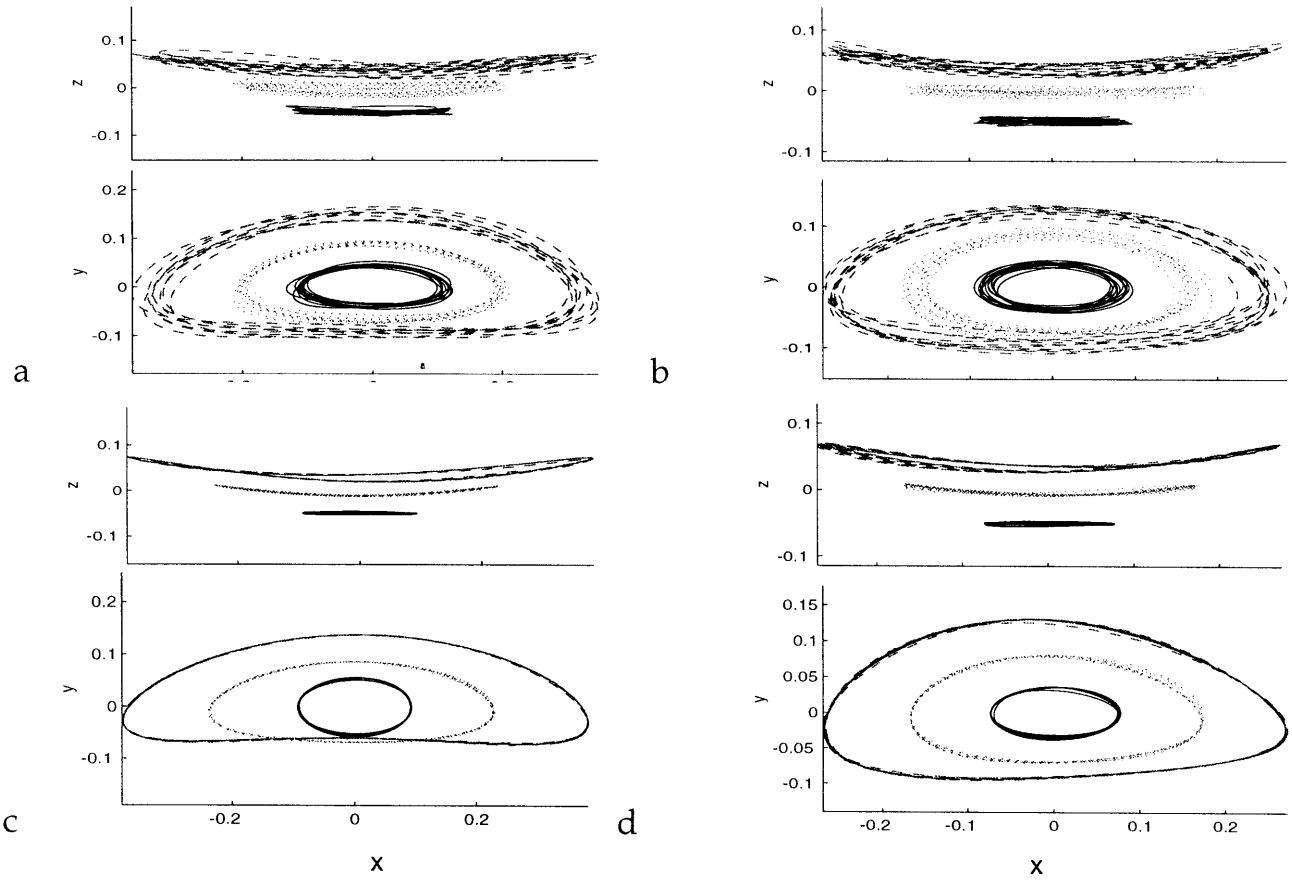

Fig. 4a–d Spatial realization of the elliptical patterns. Each plot shows two orthogonal projections of a small, medium, and large elliptical trajectory after the patterns were aligned at their means and rotated into the principal component coordinate frame. Note that in the *x*–*z* projection, the patterns were manually offset by 0.05 m to enhance the discriminability of the three pattern sizes. **a** Human frontal, **b** human oblique, **c** robot frontal, **d** robot oblique

lipse, the uniform slope *k* appears to indicate one movement segment, in agreement with Viviani and Cenzato (1985). However, for larger ellipses the single slope splits into two slopes, suggesting two segments. It is worth noting that this splitting into a V-shape happens gradually with increasing size of the ellipse. A quantification of this gradual splitting is given by the R^2 values of the "power law" fit, which decreases significantly with increasing deviation from a single linear fit. The R^2 values for all subjects for the smallest and the largest ellipses in both the frontal and oblique orientation are included in Table 2. These data seem to demonstrate that ellipses in frontal orientation have one or two segments, depending on the size, or that they always consist of two segments whereby the second segment only becomes visible for larger patterns. Following the logic that different *k*'s indicate different movement strokes, this gradual appearance of a "segmentation" is a contradiction in terms. As it correlates with size variations of the involved arm movements, one might rather suspect that nonlinearities in the forward transformation of the arm kinematics increasingly contribute to this distortion, a conjecture which will be expanded in the discussion section.

Table 2 Exponents β and their coefficients of determination obtained from fitting the power law of the tangential velocity against radius of curvature in the five subjects' data

	Frontal orientation				Oblique orientation			
	Exponent β		R^2		Exponent β		R^2	
	Small	Large	Small	Large	Small	Large	Small	Large
Subject 1	0.31	0.25	0.90	0.70	0.32	0.22	0.83	0.70
Subject 2	0.30	0.25	0.93	0.70	0.33	0.28	0.93	0.78
Subject 3	0.32	0.34	0.88	0.83	0.34	0.21	0.86	0.63
Subject 4	0.31	0.16	0.94	0.64	0.31	0.30	0.86	0.73
Subject 5	0.31	0.25	0.92	0.53	0.32	0.22	0.78	0.68

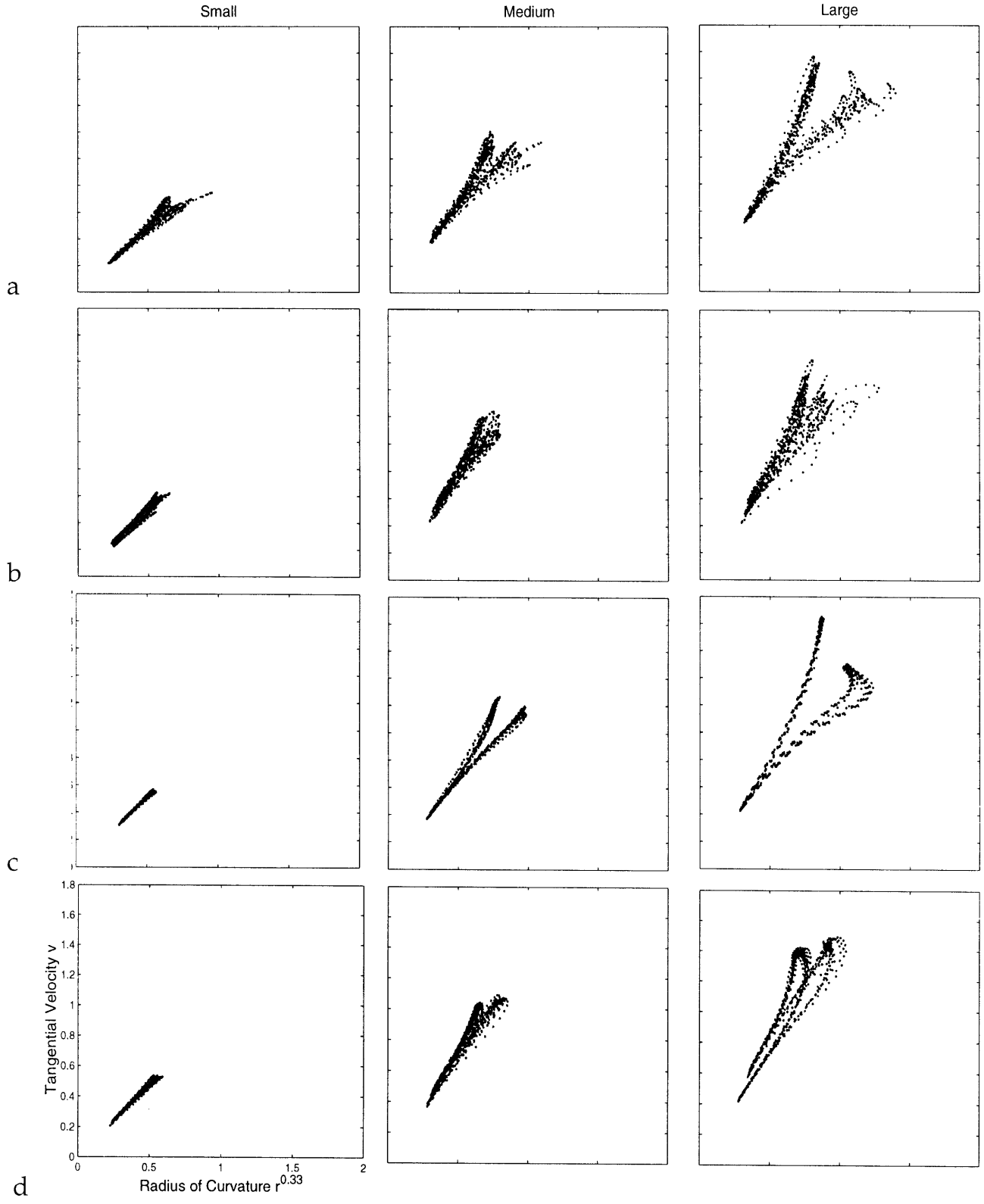

Fig. 5a–d Tangential velocity versus radius of curvature to the power of 1/3 for ellipses of small, medium, and large size for both pattern orientations corresponding to trajectories in Fig. 4a, human frontal; Fig. 4b, human oblique; Fig. 4c, robot frontal; Fig. 4d, robot oblique

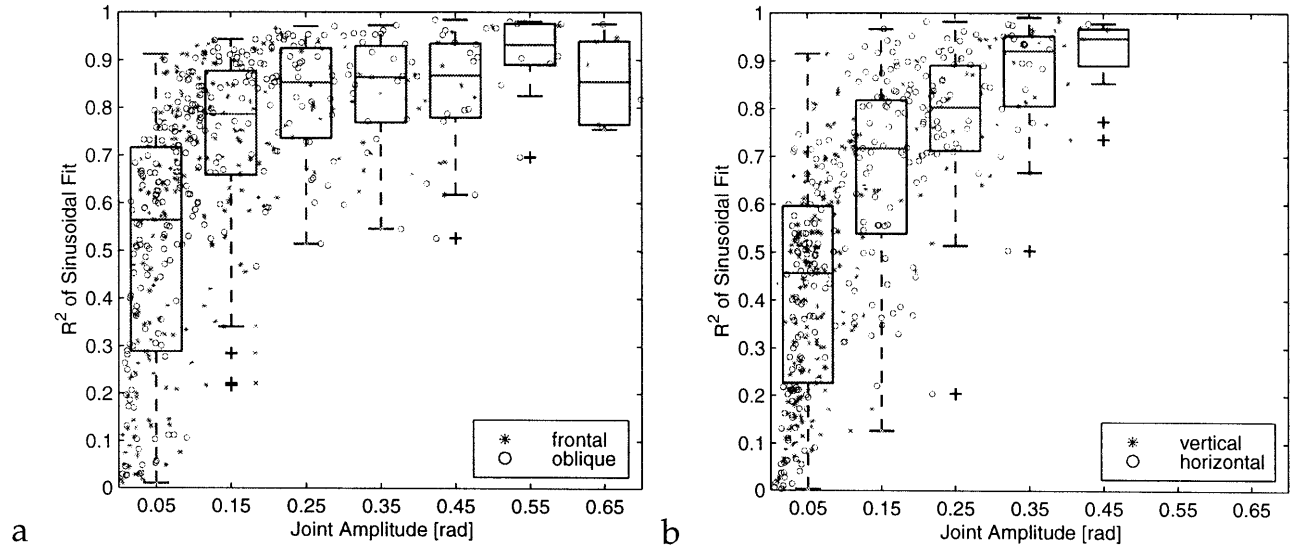

Fig. 6 Coefficients of determination for sinusoidal fits for all trials of all subjects for **a** elliptical patterns, **b** figure eight patterns. The individual data points are additionally superimposed with box plots. To generate the box plots, the coefficients of determination were binned at 0.05, 0.15, 0.25, 0.35, 0.45, 0.55, and 0.65 rad with a bin width of 0.1. The *lower end of each box* indicates the 25% quartile of the data in the bin, the *upper end* the 75% quartile, and the *horizontal line in the box* the median. The median is a robust estimator of the average sinusoidal fit quality as a function of the joint amplitude. The *"whiskers" of each box*, indicating the spread of the data in each bin, are calculated as 1.5 times the interquartile range. The *plus signs* indicate outliers. See Huber (1981) for more details

Figure 5b shows the *v–r* plots of one subject performing oblique elliptical patterns. Again, the V-shape appears in larger-sized ellipses, but in a less pronounced manner. An explanation for these data and the difference with respect to the frontal orientation will also be provided in the Discussion.

Joint angle trajectories

After converting the marker data into joint angle trajectories, all time series of the seven joint angles were fitted by sinusoids. Figure 6a summarizes the R^2 values of all sinusoidal fits for the elliptical patterns. Figure 7 shows typical cases of joint trajectories together with their sinusoidal fits. By manual inspection of all subjects' individual trajectories, we determined five different categories. The most frequent case was when sinusoids fitted the trajectories with high R^2 values as shown in Fig. 7a (31% out of 1400 trajectories, including figure eight patterns). In 15% of the data, a slow frequency drift was observed which usually occurred at the end of a block of trials indicating first signs of fatigue in the subjects. Although the drift reduced the R^2 values, it had no significant impact on the quality of the reconstruction of the patterns (Fig. 7b). Figure 7c shows a trajectory with low angular amplitude that had an additional structure beyond the sinusoidal base pattern, an effect observed in about 28% of the trials. It is hard to identify the cause of these higher order frequency patterns[2]. The fourth class of joint angle trajectories (7%) had a reduced amplitude and showed contamination by interaction torques. Figure 7d depicts an example of a figure eight trial in which a joint angle oscillates at twice the fundamental frequency. The irregularities in this trajectory are due to the acceleration peaks of other arm degrees of freedom oscillating at the fundamental frequency. A last class of angular trajectories (19%) had no significant amplitude, indicating a joint angle that was not used for the pattern.

It would have been possible to make the data fitting more accurate and allow for varying amplitude or frequency parameters or more elaborate oscillator models. This, however, would have defeated the purpose of our research. The goal was to accomplish a simple continuous movement primitive which can generate movement patterns at particular workspace locations such that qualitative shape of the human trajectories could be repeated. In all trials, it was possible to faithfully reproduce the main effects of the human movement with this simple sinusoidal model, as the figures and tables below demonstrate.

Descriptive kinematics of the endpoint trajectory of the robot

The robot implementation was performed using the modeled set of amplitudes, frequencies and phases regressed from the seven joint angles across the different pattern

[2] One possibility could be interaction torques, but our recording technique is also likely to contribute to these patterns: Since the markers attached to the subjects' arms are significantly offset relative to the neutral axis of the limb, even single degree of freedom movement causes motion in several markers that will be interpreted as if several degrees of freedom were moving. This spurious movement reduces the signal-to-noise ratio, particularly for small angular amplitudes. Since such trials had typically much lower amplitude than the other contributing degrees of freedom, their effect on shape of the pattern was minor, as we confirmed in simulations.

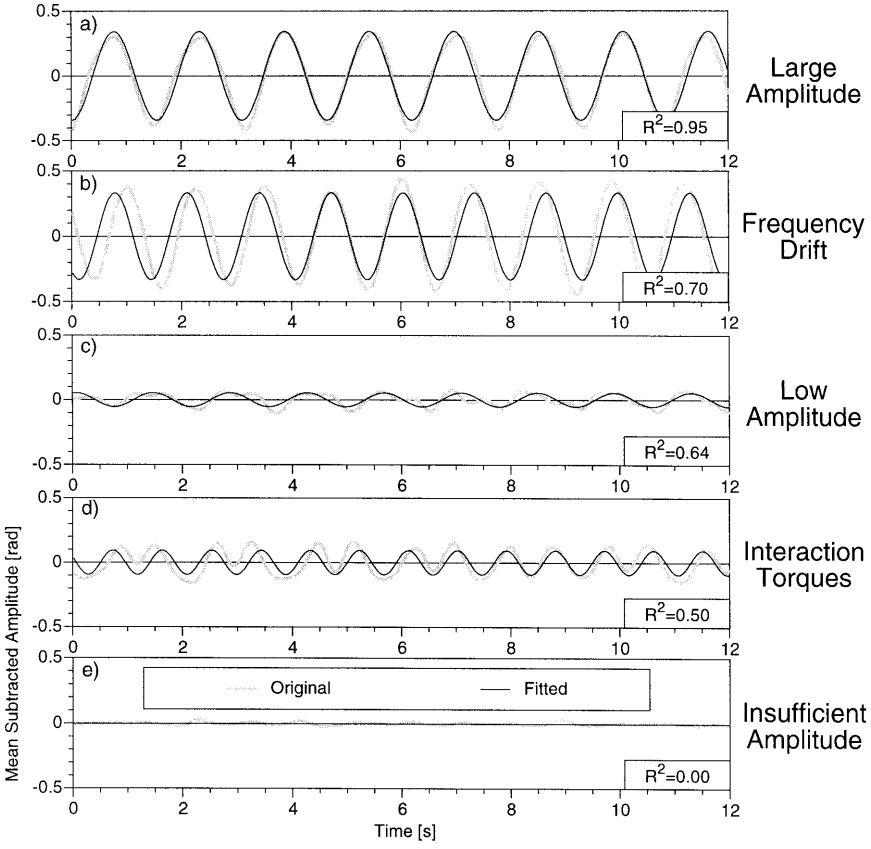

Fig. 7a–e Representative examples of sinusoidal approximations of joint angle trajectories. The original trajectories are shown as *dimmed lines*, the fitted ones as *solid black lines*. The five graphs illustrate five typical categories determined from the 1400 joint angle trajectories of all subjects across all degrees of freedom for both figure eight and elliptical patterns. These categories were: **a** large-amplitude patterns usually associated with high R^2 values: 31%; **b** slowly drifting frequency patterns usually having reduced R^2 values: 15%; **c** low-amplitude trajectories (low signal-to-noise ratio): 28%; **d** trajectories contaminated by interaction torques: 7%; **e** trajectories with no significant amplitude: 19%

sizes of each subject. Figure 4 provides a comparison of human and robot data for the same representative subject and trajectories. Since the robot data were collected in the same way as the human data using the visual motion tracker, some scatter of the repeated bands exists as a result of measurement noise. The figure also illustrates that the overall shapes of the ellipses reproduced by the modeled data are approximately congruent with the human ones, although the largest pattern of the robot in oblique orientation shows stronger deviations from a pure ellipsoid than the human data.

The descriptive data of the robot's endpoint trajectories are summarized in Table 3. The data show similar trends in all measures as the human data, although sometimes in a more pronounced fashion. Most noteworthy is the fact that the R^2 values of the power law fit decrease significantly from the small to the large patterns in both orientations (frontal $t(4)=5.4$; $P<0.005$; oblique $t(4)=5.7$; $P<0.004$). It should be pointed out that perimeter differences between the human and robot data are due to the differences in arm length between subjects and robot.

An additional measure to evaluate the congruence of human and robot data, the height/width ratio of the ellipses of all sizes, was determined. As summarized in Table 4, the mean width/height ratio of the ellipses was statistically indistinguishable from the human data in seven out of ten pattern sequences; in three cases (S4-frontal, S1-oblique, S3-oblique) the mean showed a small but statistically significant offset. For the purpose of our research, however, these offsets are of minor importance since all

Table 3 Kinematic measures of the smallest and largest of the ten elliptic patterns in frontal and oblique orientation performed by the robot using the modeled data of the five subjects

	Frontal orientation				Oblique orientation			
	Perimeter (m)		Planarity (m)		Perimeter (m)		Planarity (m)	
	Small	Large	Small	Large	Small	Large	Small	Large
Subject 1	0.625	2.092	0.003	0.012	0.435	0.944	0.001	0.006
Subject 2	0.479	1.649	0.002	0.017	0.354	1.289	0.001	0.014
Subject 3	0.409	1.349	0.003	0.013	0.242	0.940	0.000	0.004
Subject 4	0.403	1.638	0.000	0.007	0.365	1.295	0.001	0.018
Subject 5	0.341	1.917	0.000	0.004	0.459	1.243	0.001	0.007

Table 4 Comparison of mean width/height measures for human and robot trajectories [*one outlier removed (P>0.95)]

	Frontal orientation				Oblique orientation			
	Human		Robot		Human		Robot	
	Width/height		Width/height		Width/height		Width/height	
	Mean	SD	Mean	SD	Mean	SD	Mean	SD
Subject 1	0.354	0.050	0.324	0.071	0.614	0.043	0.855	0.023
Subject 2	0.386	0.020	0.386	0.121	0.458	0.024	0.442	0.021
Subject 3	0.507	0.030	0.441*	0.044	0.650	0.072	0.858	0.043
Subject 4	0.368	0.023	0.279	0.009	0.709	0.044	0.662	0.035
Subject 5	0.268	0.049	0.211	0.060	0.442	0.076	0.384	0.126

Table 5 Fitted exponents and their coefficients of determination obtained from nonlinear regression of the tangential velocity against radius of curvature in the robot's data modeling the five subjects' data

	Frontal orientation				Oblique orientation			
	Exponent β		R^2		Exponent β		R^2	
	Small	Large	Small	Large	Small	Large	Small	Large
Subject 1	0.31	0.19	0.93	0.42	0.28	0.14	0.73	0.36
Subject 2	0.33	0.24	0.99	0.65	0.33	0.29	0.98	0.84
Subject 3	0.33	0.24	0.83	0.68	0.30	0.25	0.70	0.31
Subject 4	0.30	0.15	0.94	0.36	0.32	0.30	0.94	0.59
Subject 5	0.32	0.26	0.98	0.50	0.29	0.25	0.90	0.70

Table 6 Kinematic measures of the thinnest and widest of the ten figure eight patterns performed in horizontal and vertical orientation by five subjects

	Horizontal orientation						Vertical orientation					
	Perimeter (m)		Width/height (m)		Angle (rad)		Perimeter (m)		Width/height (m)		Angle (rad)	
	Thin	Wide	Thin	Wide	Thin	Wide	Thin	Wide	Thin	Wide	Thin	Wide
Subject 1	1.299	2.803	0.04	0.65	0.53	1.01	1.119	2.056	0.03	0.86	0.35	0.42
Subject 2	1.451	2.503	0.04	0.85	0.47	0.61	0.950	1.672	0.03	0.89	0.25	0.61
Subject 3	0.903	1.801	0.05	0.97	0.26	0.33	1.010	2.003	0.03	0.91	0.29	0.69
Subject 4	1.198	2.286	0.03	0.73	0.44	0.60	1.260	1.891	0.02	0.52	0.40	0.48
Subject 5	1.103	3.067	0.03	0.91	0.42	0.73	1.169	2.992	0.03	0.96	0.15	0.38

that mattered was that a series of ellipses with the same orientation was repeated in the same workspace location as in the human data.

Power law and velocity gain factor in the robot data

Table 5 summarizes the results of the power law regression analysis performed on the robot's data. Again, the exponent of the small patterns is strikingly close to the expected value of 1/3, whereas there is considerable deviation in the largest patterns. This trend is accompanied by a significant decrease in the R^2 values. Figure 5c,d shows the *v*–*r* plots of the robot's realization of the subject's ellipses. Conspicuously, the emergence of the V-shape with increasing pattern size is even clearer and reveals a fine structure that has not been seen in the subject's data. Also similar to the human data, the change into a V-shape is more pronounced in the frontal than in the oblique pattern. Following the argument developed in the literature on the power law, these observations suggest that, while a small ellipse might be generated by only one movement segment, the larger ellipses should consist of two segments. Such a conclusion is in contradiction to the known fact that the robot implements a set of purely sinusoidal joint displacements for the complete set of elliptic patterns, and requires the search for alternative explanations, as provided in the "Discussion."

Figure eight patterns

Descriptive data

Table 6 provides an overview of the descriptive kinematic measures of the horizontal and vertical ellipses for each of the five subjects. The mean perimeter, width/height ratio, and the angle between the two lobes of the

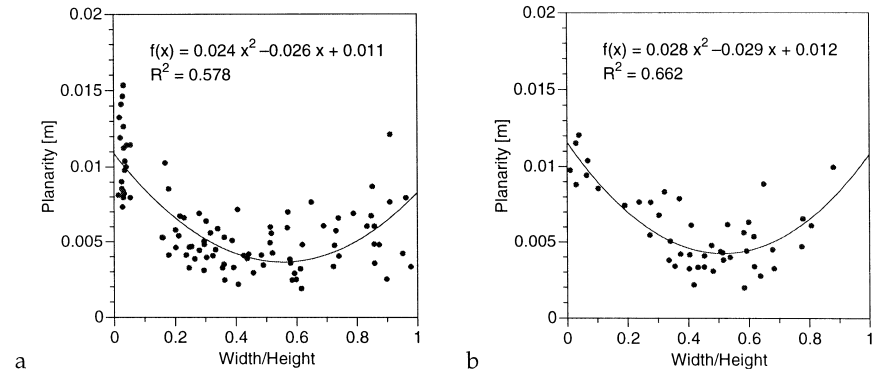

Fig. 8a, b Planarity of the figure eight patterns as a function of the width/height ratio of the pattern, pooled across both the horizontal and vertical pattern of all subjects: **a** human data, **b** robot data

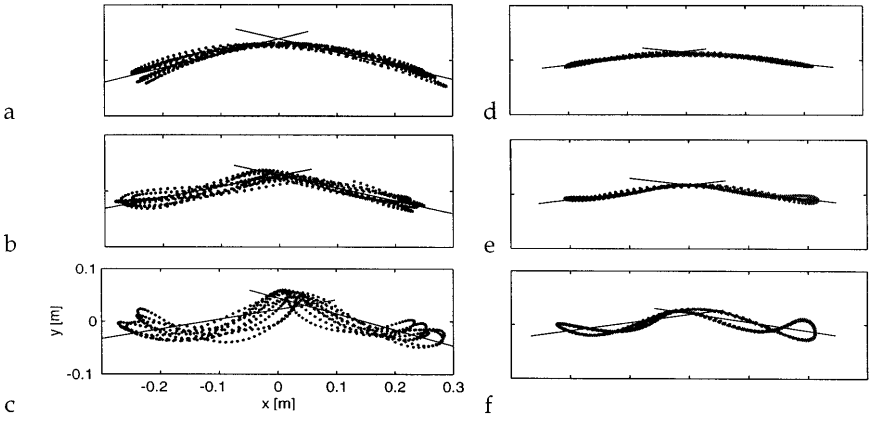

Fig. 9a–f Planar projection of one subject's figure eight patterns of small, medium, and large width/height ratios: **a–c** human data, **d–f** corresponding robot data

figure eight are listed for the smallest and the largest figure eight. As can be seen from the table, the perimeters increase approximately 2–3 times the size of the small figure eight. The width/height ratio spans the whole range between 0 and 1, as specified in the experimental task. Importantly, the angle between the principal component planes of the two figure eight lobes increases as a function of the pattern size. No difference could be found in the descriptive measures between the horizontal and vertical figure eight patterns.

Planarity

Figure 8a illustrates how the planarity of the figure eight patterns varies as a function of the width/height ratio: planarity decreases with width/height ratios from zero towards a ratio of 0.5, and then increases again. This means that when the width/height ratio ≈0.5, corresponding to lobes which are approximately circular, the two lobes are best confined to a plane. A quadratic regression confirmed the high significance of this trend ($p<0.0001$). The reason for this trend becomes apparent when inspecting the subjects' patterns in a projection where the principal component planes of both lobes look like lines, i.e., the angle between the planes is undistorted. Figure 9a–c illustrates this projection for one representative subject performing a figure eight pattern with a small, medium, and large width/height ratio. The projected planes are superposed onto the data as lines. Small-width figure eight patterns (Fig. 9a) look rather curvilinear, reflected in a larger planarity value. Medium-width patterns (Fig. 9b) are convincingly piecewise planar, reflected in a small planarity value. However, large-width figure eights (Fig. 9c) show a curved trend in each of the lobes, yielding a higher planarity value. Soechting and Terzuolo (1987a) suggested that this curvature in larger sizes indicates four movement segments in the figure eight, while for the medium width/height ratio, experimental evidence indicates only two segments. Given the continuous transition of the planarity value as a function of the width/height ratio, we will argue below that the observed phenomena may be due to the specific kinematic configuration of the human arm, and not necessarily to a segmented central planning strategy.

Joint angle data

Figure 6b shows the R^2 values of all sinusoidal fits in the five subjects as a function of the amplitudes of the sinusoids. The results are similar to those in the elliptical patterns in Fig. 6a. Since in figure eight patterns some joint angles need to oscillate at twice the base frequency of the pattern, the joint angle trajectories showed some additional contamination from interaction torques. These effects caused the generally slightly decreased quality of fit of the sinusoids, as apparent in Fig. 6b.

Table 7 Kinematic measures of the thinnest and widest of the ten figure eight patterns in horizontal and vertical orientation performed by the robot using the modeled data from the five subjects

	Horizontal orientation						Vertical orientation					
	Perimeter (m)		Width/height (m)		Angle (rad)		Perimeter (m)		Width/height (m)		Angle (rad)	
	Thin	Wide	Thin	Wide	Thin	Wide	Thin	Wide	Thin	Wide	Thin	Wide
Subject 1	1.674	2.360	0.03	0.37	0.50	0.63	1.530	2.049	0.04	0.53	0.50	0.58
Subject 2	1.327	2.160	0.04	0.58	0.37	0.47	0.888	1.469	0.01	0.67	0.40	0.60
Subject 3	0.649	1.159	0.04	0.77	0.16	0.40	0.751	1.374	0.03	0.60	0.33	0.40
Subject 4	1.152	2.198	0.03	0.61	0.41	0.52	1.433	2.006	0.03	0.45	0.44	0.55
Subject 5	0.865	1.536	0.03	0.88	0.23	0.48	1.014	1.705	0.04	0.65	0.44	0.54

Descriptive data of the robot

The human data were modeled and implemented on the robot in the same manner as for the elliptical patterns. As for the elliptical patterns, the robot produced qualitatively similar effects in the descriptive data as the human subjects, summarized in Table 7.

Planarity of robot data

Figure 8b demonstrates that the robot's dependence on the planarity measure as a function of the width/height ratio follows essentially the same trend as in the human data. In particular, as evident in Fig. 9d–f, the segmentation characteristics according to piecewise planarity are reproduced by the robot. As the robot was guaranteed to use an unsegmented control strategy, these results are at odds with the hypothesis that piecewise planarity reflects segmented control.

Discussion

The results of our experiments revealed that kinematic features like piecewise planarity and discontinuities in the velocity gain factor of the two-thirds power law, which have been interpreted as indicators for segmentation, can be generated by a continuous unsegmented control strategy. While these findings in both human and robot data empirically cast doubt on the hypothesis of stroke-based control for the chosen patterns, the question of which other mechanisms cause such "spurious" segmentation at the level of endpoint movements is still unanswered. In the following it will be argued that the nonlinear transformations added to joint angle trajectories by the forward kinematics transformation of human arms are responsible for these systematic kinematic features at the endpoint.

An explanation for changes in the velocity gain factor

To illuminate the effects observed in the velocity gain factor we performed a simulation with a planar two-joint arm which executed elliptical endpoint trajectories. Figure 10a shows a sketch of the arm whose state is described by the angles θ_1 and θ_2. The simulation was driven by sinusoidal motions for both joint angles, $\theta_1=A_1 \sin(\omega t)+\theta_{1,0}$, $\theta_2=A^2 \sin(\omega t+\varphi)+\theta_{2,0}$. The angular amplitudes of the joint angles were A_1 and A_2, the angular frequency was ω, the angular zero offsets were $\theta_{1,0}$ and $\theta_{2,0}$, and the phase offset between the two oscillations was φ. The two-joint arm, with a forearm length of 0.4 m and an upper arm length of 0.3 m, traced one cycle in the frontal and oblique ellipsoidal pattern (at 60 Hz), producing a small- and a large-sized ellipsoid in each orientation. Cartesian coordinates of the arm's endpoint trajectories were calculated using the standard forward kinematics equations (e.g., Atkeson 1989). From these data, the radius of curvature and the tangential velocity could be computed (Lacquaniti et al. 1983). Figure 10a,c illustrates the spatial realization of these patterns, while Fig. 10b,d depicts the *v–r* plots analogous to Fig. 5. The small and the large cyclic patterns are superimposed in each plot and, additionally, the two minima and maxima of the curvature are marked by the numbers 1–4.

When comparing the *v–r* plots of the simulated arm with the human and robot data in the frontal orientation (Fig. 10b vs Fig. 5a,c), and in the oblique orientation (Fig. 10d vs Fig. 5b,d), it becomes apparent that the two-joint arm simulation captures the major effects observed in the experimental data. While for small ellipses the *v–r* plots display a uniform slope, for large ellipses an additional structure emerges. For the frontal patterns the V-shape in the *v–r* plot becomes significant, and even the additional "kink" in the right branch of the *v–r* pattern is reproduced in the simulation (Fig. 9b). In contrast, the oblique pattern has a less-pronounced V-shape, but the branches develop a "sling" at higher tangential velocities, just as observed in human and robot data. It was surprising how well the 2-DOF simulation also reproduced various features of the human and robot 7-DOF trajectories in Fig. 4, in spite of the strongly reduced dimensionality of this simulation.

To explain the effects in the *v–r* plots it helps to trace one cycle of the elliptical patterns together with its associated branches in the *v–r* plot. As Viviani and Cenzato (1985) noted, the slope of a branch in the *v–r* plot is related to the average tangential velocity of a movement segment. For the small ellipses, which were typically in-

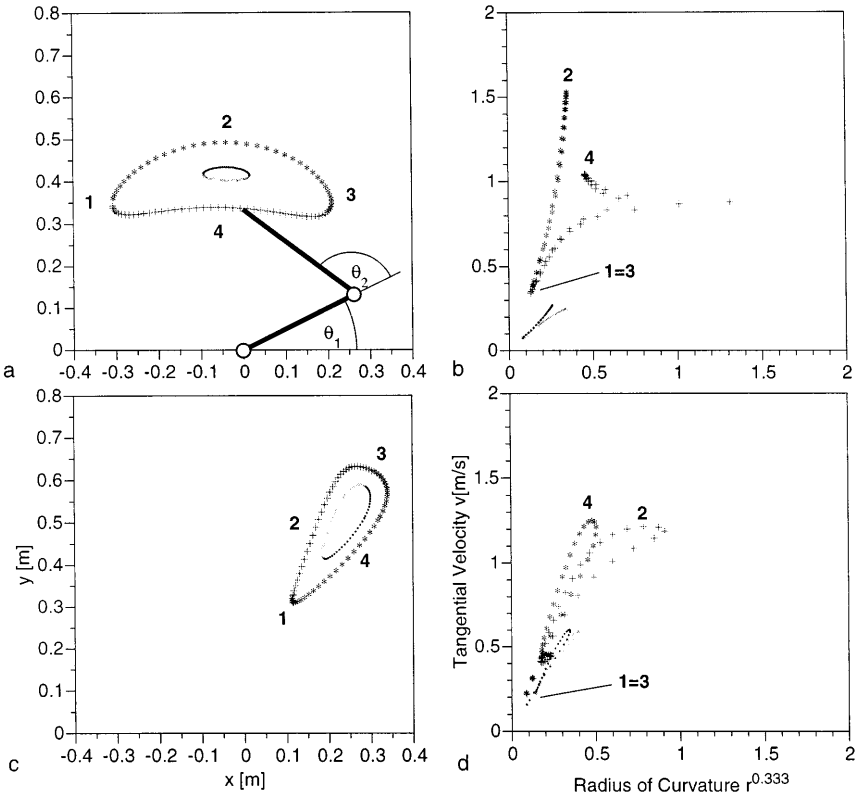

Fig. 10a–d Two-joint arm simulation of frontal and oblique ellipsoidal pattern in two sizes. **a** Frontal ellipses ($\theta_{1,0}$=0.5, $\theta_{2,0}$=1.9, φ=2.2, ω=4.7; large: A_1=0.75, A_2=0.3; small: A_1=0.15, A_2=0.06); **b** corresponding *v–r* plot; **c** oblique ellipses ($\theta_{1,0}$=0.4, $\theta_{2,0}$=1.25, φ=3.34, ω=5.6; large: A_1=0.57, A_2=0.95; small: A_1=0.3, A_2=0.5); **d** corresponding *v–r* plot. The *numbers at the large ellipses* mark the points of maximal and minimal tangential velocity; the corresponding points are shown in the *v–r* plots

vestigated in two-thirds power law studies, the average tangential velocities for the arcs demarcated by the curvature extrema shown in Fig. 10 are not significantly different – the entire ellipse therefore appears to have one constant velocity gain factor. But when the pattern size is successively increased as in our experiment, the nonlinearities of the arm kinematics come to bear and emphasize the deviations of the large patterns from symmetric ellipses. For instance, in Fig. 10a the endpoint of the arm travels a larger distance in the more distal arc of the ellipse than in the more proximal one, while the time to traverse either branch is the same. Thus, the average velocity for the distal branch is higher and, consequently, results in a different *k* value; this effect generates the second branch in the *v–r* plot. The additional kink for the large ellipse in Fig. 10b results from a transition from convex to concave curvature. Also the differences in the *v–r* plots between the frontal and oblique patterns now become understandable. For the frontal pattern, the two points of minimal tangential velocity (1, 3) demarcate the distal (i.e., high-velocity) from the proximal (i.e., low-velocity) arc of the ellipse. In contrast, due to its different orientation, the oblique ellipse's tangential velocity is less symmetric. Starting at the ellipses' proximal point in Fig. 10c, the first quarter of the ellipse is traversed at a slower average velocity than the second more distal quarter. These differences result in the "sling" in Fig. 10d. Traversing the third and fourth quarters of the ellipse, the same effect happens, but since the ellipse is not symmetric, a slightly different "sling" is formed.

Upon closer inspection of the congruence of human and simulation patterns, it is interesting that while the ellipses in the frontal orientation (Fig. 10a) are very similar to human patterns in Fig. 4a, the ellipses in the oblique direction (Fig. 10c) appear to differ more significantly from human patterns (Fig. 4c) although their *v–r* plots are strikingly similar. This difference can be explained by inspecting the way subjects achieved the patterns. For the frontal ellipses, subjects used their arm degrees of freedom similar to the 2-DOF arm, i.e., they generated a horizontally lying ellipse primarily out of the motion of one shoulder and one elbow degree of freedom. For the oblique ellipses, subjects distributed their motion more equally over the four proximal degrees of freedom, i.e., SFE, SAA, HR, EB (Fig. 3). Moreover their patterns were no longer exactly horizontal but rather they were tilted in a plane that inclined radially towards the distal parts of the workspace. However, these shape differences do not affect the main features of the velocity distribution that lead to the "slings" in the *v–r* plots.

In sum, the simulation using the simplified two-joint arm corroborated the main point that none of the effects in the *v–r* plots are due to a segmented strategy. Although the simulated two-link system is far from the complex 7-DOF human arm, it is important to emphasize that this simulation is simple enough to allow a complete explanation for these features based on the nonlinear kinematics of the human arm.

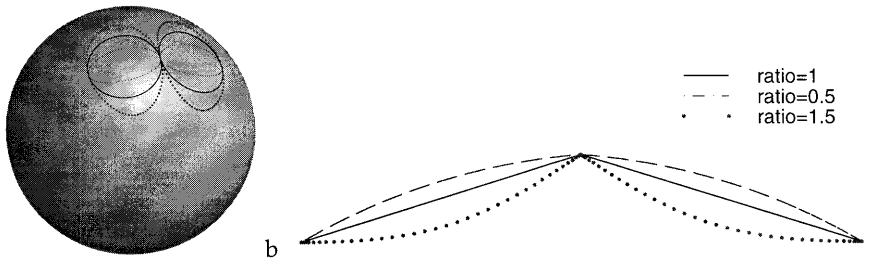

Fig. 11 Endpoint trajectories of the "gedanken arm" generated by two sinusoidal joint movements: **a** Trajectories lying on a sphere; **b** lateral projections of the figure eights result in the same shapes as in human data

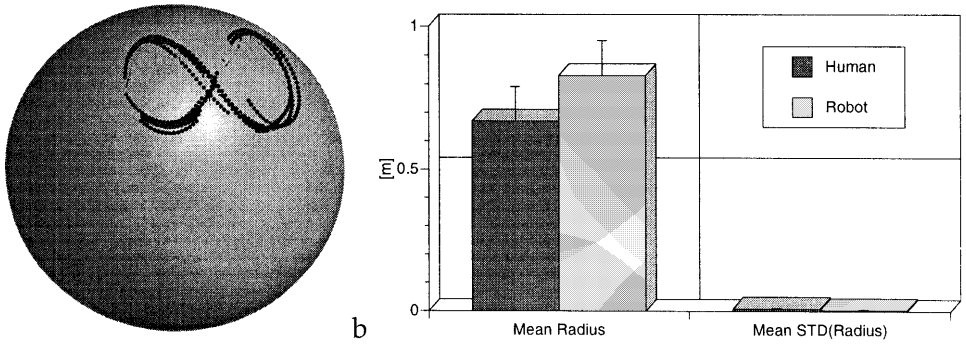

Fig. 12 **a** Figure eight pattern of a representative subject superimposed on the fitted sphere (note that data points inside the sphere are hidden by the opaque surface); **b** mean and standard deviations of the spherical fits across all subjects (note that the bars are hardly visible since they are so short)

An explanation for piecewise planar units

A simple example may give an intuitive explanation of how piecewise planar segmentation can arise from continuous control. Imagine a "gedanken arm" with only one link of length L moving with 2 DOF that are described by angular coordinates corresponding to standard spherical coordinates. This arm is meant to be a simplified human upper arm moving from the shoulder joint ignoring humeral rotation and elbow or wrist joints. If both angular degrees of freedom oscillate sinusoidally with equal amplitude and a 90° phase offset, the endpoint of the arm will trace a circular pattern. This circular trajectory will lie in a perfect plane, but, of course, also on a sphere with radius L. A figure eight pattern can be obtained by connecting two such circular patterns in a continuous trajectory, which can be accomplished when the frequencies of the 2 DOF are in a 1:2 ratio. Assuming a 1:2 ratio in amplitudes – the slow degree of freedom has twice the amplitude of the fast degree of freedom – the two lobes of the figure eight will be approximately circular and will lie in different planes – imagine cutting off two equal-sized slices from a sphere such that the slices just touch each other. Thus, tracing a figure eight with the gedanken arm will generate piecewise planar endpoint trajectories, despite the fact that the trajectory is generated by two continuous oscillations. If the amplitudes of the two oscillations change and have a ratio different from 0.5, the generated figure eights will become "stretched" or "squashed" similar to the experimental patterns (Fig. 11a). When looking at the lateral projections of such generated figure eight patterns (Fig. 11b), the same linear and curvilinear shapes appear as seen previously in the experimental trials shown in Fig. 9: For an amplitude ratio of 0.5 (corresponding to a width/height ratio of 0.5 for the experimental figure eights), perfect piecewise planarity exists. For an amplitude ratio of 0.25 (width/height=0.25), the projection looks like one convex arc. For an amplitude ratio of 0.75 (width/height=0.75), the projection looks like two concave arcs.

Can these simulation results of a 2-DOF gedanken arm be generalized to a full 7-DOF arm? To address this question we investigated whether the endpoint trajectories of human subjects and the robot lay on a spherical surface. To this end, the best spherical fit for each figure eight was approximated by minimizing the sum squared error of $(R^2-((x_i-x_0)^2+(y_i-y_0)^2+(z_i-z_0)^2))$, where the origin of the sphere is defined at (x_n,y_0,z_0) and its radius is R. Each data point of the arm's endpoint trajectory is denoted by (x_i,y_i,z_i), and $R^2=\text{mean}((x_i-x_0)^2+(y_i-y_0)^2+(z_i-z_n)^2))$. Using Levenberg-Marquardt nonlinear regression, we obtained R and (x_n,y_0,z_0). The result revealed that both the subjects' and the robot's figure eight trajectories indeed lay remarkably well on a spherical surface. Since this fitting procedure does not return an R^2 value in the traditional regression sense, the results are best expressed by the mean of the standard deviations of the approximated radii of all spherical fits for all pattern sizes and all subjects; the mean was 0.008 m for the subjects and 0.004 m for the robot's trajectories. This was extremely small compared to the mean radii of the spheres (across all trials and subjects): 0.67 m for the human subjects and 0.83 m for the robot. Figure 12 gives a representative example of the figure eight of one subject superimposed on the fitted sphere, as well as the spherical fit statistics across all subjects.

Thus, the observed realizations of the figure eight patterns seem to be accounted for by one explanation: a continuous, approximately sinusoidal control strategy in joint space that generates endpoint trajectories which lie approximately on a sphere. No segmentation needs to be

hypothesized to account for the observed phenomena. Furthermore, there is no need to suggest different segmentation within the same pattern, as Soechting and Terzuolo (1987a,b) required to account for some figure eights with two segments, and for others with four segments. Piecewise planarity of the endpoint trajectory can be a by-product of the kinematic chain of human arms. However, our data also demonstrated that the effect of piecewise planarity can be less convincing for especially chosen patterns, as was shown for the very slim and the "squashed" figure eights (Fig. 9).

The inevitable question following from these results is why should the endpoint trajectory of a 7-DOF arm be confined to a spherical surface – clearly, the trajectories of a 7-DOF arm can lie on much more irregular surfaces. As a first hypothesis one could assume that the subjects moved their arms primarily out of the two major shoulder joints (SFE, SAA, cf. Fig. 3), thus reducing their 7-DOF essentially to the 2-DOF gedanken arm. Our data, however, reject this hypothesis since (a) also HR and EFE have amplitudes comparable in magnitude to SFE and SAA, and (b) the center of the fitted spheres is on average (across all subjects and conditions) 0.14 m (SD=0.056 m) away from the shoulder marker (cf. Fig. 1), thus discounting the shoulder as the sole center of the arm movements. We therefore conjecture that the surface generated by the endeffector is of some complicated concave or convex nature, which, due to the moderate amplitudes of the joint movements, is well approximated by a sphere in the range the data was generated. Moreover, particular phase relationships among the joint angles can help making the endeffector movement more spherical, even perfectly spherical in spite of large joint angle amplitudes. Well-designed experiments should be able to predict under which conditions the endeffector data become less spherical. A further elaboration of this issue, however, is beyond the scope of the present study and will be addressed in subsequent investigations.

Choice of reference system

Some additional aspects of our results and experimental procedure need to be addressed with respect of the extant literature. The first issue is the choice of the coordinate frame that we used to describe the angular positions of the human arm. While we chose a biomechanical coordinate system (Wood et al. 1989) that can be directly translated into simulations and implementations in robotic hardware, the work of Soechting and colleagues was rooted in a more abstract, psychologically motivated reference system, defined to describe 4 DOF. Soechting and Ross (1984) argued in favor of their choice of coordinates on the basis of a "matching experiment" in which they examined how well subjects could blindfoldedly match certain orientation angles of their right arm with their left arm. Would an analysis of our data in terms of this coordinate system change our results? The only difference of such a change of coordinates would be in terms of the sinusoidal fits of the joint angle trajectories. Assuming that the Soechting and Ross coordinate system is more adequate, we would obtain an improved reproduction of the human behavior with the robot, as argued by Soechting and colleagues (Soechting and Terzuolo 1986; Soechting et al. 1986). Since the robot data already reproduced the features of human movement, it is unlikely that an even better reproduction would change any of our statements. Given the redundant and complex arrangement of muscles in a human arm, it is quite unlikely that there is a single joint angle coordinate system that can properly reflect the planning of the CNS – it is more likely that the CNS has a continuum of coordinate systems for arm movements, implicitly expressed by which muscle synergies are currently used in a task. Using variables as defined in Fig. 3 can only be an approximation to capture the main effects of the joint angle movement, but it is not a suggestion that the CNS uses these variables. It is very likely that for different movement tasks, different choices of joint coordinate systems need to be made in order to accomplish a parsimonious and useful description of arm movements.

Disagreement with EMG data

Given the goal of the present investigation, it is noteworthy that despite the proposed segmentation of figure eight patterns in Soechting and Terzuolo (1987a, p. 46), the EMG data collected in respective muscle groups showed no signs of this segmentation. While the authors concluded that EMG data are not adequate for detecting movement segmentation, our results suggest that the EMG traces may properly reflect the underlying continuous control strategy.

Segmentation in nonrhythmic patterns

Soechting and Terzuolo (1987a,b) also examined more complex movement patterns, including self-paced irregular scribbles, and identified piecewise planar elements. Our explanation for these results directly connects to the arguments developed around Fig. 11: If the endeffector movement of a human arm approximately lies on a sphere for extended parts of the workspace, and if the pattern largely consists of circular slings – as is suggested by the plots of Soechting and Terzuolo (1987a,b) – one would expect to be able to approximate the movement with piecewise spherical surfaces on which the trajectory pieces will be approximately piecewise planar, as exemplified in Fig. 11b. Of course, this argument does not say that scribbles result from an unsegmented control strategy – just the fact of piecewise planarity as indication for segmentation may have to be discounted. One extension of our argument could be that scribbles are generated by oscillatory pattern generators in joint or muscle space whose amplitudes, frequencies, phases, and rest angles are changed rapidly at certain times. It is

highly likely that this control strategy would generate piecewise planar trajectories as we confirmed in preliminary simulation and robot studies. On the other hand, piecewise planarity does not always have to emerge in three-dimensional movement, as was evident in our data of figure eights that had width/height ratios significantly different from 0.5, and of large elliptical patterns. Indeed, some plots in Soechting and Terzuolo (1986) and Soechting et al. (1986) indicate similar trends, although the authors did not quantify planarity.

Effects of biomechanical and muscular properties

In a simulation study using a two-jointed arm with muscle-like spring properties in the actuators, Gribble and Ostry (1996) showed that muscular and biomechanical properties can greatly alter the shape of endpoint trajectories, despite the fact that their central control signal consisted of constant velocity shifts of equilibrium points throughout the total ellipse. While their study focused on how much the musculoskeletal arm dynamics in conjunction with the equilibrium-point hypothesis can affect endpoint trajectories, our study focuses on a complementary issue, demonstrating how kinematic properties of an arm can produce segmentation features in endpoint trajectories in spite of using a continuous control strategy. It would be interesting to test to what degree alternative models of movement generation, e.g., equilibrium point models in conjunction with more biomechanically realistic arm models, can reproduce our results. Such research, however, has to wait until the appropriate movement control hypotheses have been scaled up to 7 DOF.

Piecewise planarity in isometric movements

Our results attribute the origin of piecewise planarity and discontinuous changes of k to oscillatory joint angle movements that are nonlinearly transformed by the biokinematic chain of the human arm. This explanation cannot account for the data by Pellizzer et al. (1992), who found that isometrically produced force trajectories tracing figure eight patterns in three-dimensional space seemed to have piecewise planar features, too. A discussion of this topic needs to address the differences in methods and data analysis between these isometric data and our movement data, and, in particular, the issue of when and how isometric data and real movement data are actually comparable. As for the time being such a discussion would have to speculate on some issues of the experiment of Pellizzer et al., we leave this discrepancy for a separate investigation in the near future.

Conclusions

The present study examined two hypotheses of movement segmentation in three-dimensional unconstrained drawing movements: one based on abrupt changes of the velocity gain factor of the two-thirds power law, the second based on the observation that endeffector trajectories of human arm movements tend to be piecewise planar. In both cases, our data demonstrated that the described segmentation features can equally be generated by a continuous, i.e., unsegmented, control strategy. Since these statements are based on data synthesized with an artificial movement system, i.e., an anthropomorphic robot arm whose control strategy was known to be continuous, they have the character of negative example to these hypotheses. We offered a detailed analysis of patterns over size and shape variations that highlighted the influence of the nonlinear kinematics transformations that the human arms add to the control signals generated in joint space. That the obtained analyses are relevant for human arm movement was shown in the parsimonious account that they provided for our own experimental data, but also in the context of previous work in the literature.

In the context of movement segmentation, or units of action, we suggested an account in terms of continuous oscillatory pattern generators in joint space for rhythmic drawing movements. As mentioned in the "Introduction," such a line of thought is closely related to work on central pattern generators in neurobiology and the dynamical systems' approach in psychology, while it is in contrast to ideas that arm movements are generally stroke-based and/or extrinsically planned. Oscillatory pattern generators seem to be a natural choice when generating rhythmic movement, and using them in intrinsic, e.g., joint coordinates makes the most efficient use of a movement system built from revolute joints. There are many movement tasks that explicitly exploit speed and acceleration out of joint angular movement, for instance, when cracking a whip, throwing a ball, and various kinds of racket sports. Thus, it appears that biological movement systems directly use these intrinsic variables for movement planning. An important issue in future research on motor control therefore needs to address how intrinsic and extrinsic planning can be combined task specifically (Schaal and Sternad, 1998) instead of taking extreme approaches arguing for exclusively intrinsic or extrinsic planning.

Acknowledgements The authors are grateful for the valuable remarks on earlier versions of this manuscript by Nicolas Schweighofer and Frank Pollick. This work was made possible by Award 9710312 of the National Science Foundation, the ERATO Kawato Dynamic Brain Project funded by the Japanese Science and Technology Cooperation, and the ATR Human Information Processing Research Laboratories.

References

Abend W, Bizzi E, Morasso P (1982) Human arm trajectory formation. Brain 105:331–348

Adamovich SV, Levin MF, Feldman AG (1994) Merging different motor patterns: coordination between rhythmical and discrete single-joint. Exp Brain Res 99:325–337

Atkeson CG (1989). Learning arm kinematics and dynamics. Annu Rev Neurosci 12:157–83

An CH, Atkeson CG, Hollerbach JM (1988) Model-based control of a robot manipulator. MIT Press, Cambridge, Mass
Bizzi E, Polit A, Morasso P (1976) Mechanisms underlying achievement of final head position. J Neurophysiol 39:435–444
Bizzi E, Acornero N, Chapple W, Hogan N (1984) Posture control and trajectory formation during arm movements. J Neurosci 4:2738–2744
Brown TG (1914) On the nature of the fundamental activity of the nervous centres; together with an analysis of rhythmic activity in progression, and a theory of the evolution of function in the nervous system. J Physiol (Lond) 48:18–46
Cohen MA (1992) The construction of arbitrary stable dynamics in nonlinear neural networks. Neural Networks 5:83–103
Craig JJ (1986) Introduction to robotics. Addison-Wesley, Reading, Mass
Easton TA (1972) On the normal use of reflexes. Am Sci 60: 591–599
Feldman A (1966) Functional tuning of the nervous system with control of movement or maintenance of a steady posture: II) Controlable parameters of the muscles. III) Mechanographic analysis of execution by man of the simplest motor task. Biophysics 11:565–578, 766–775
Feldman AG (1980) Superposition of motor programs. I. Rhythmic forearm movements in man. Neuroscience 5:81–90
Flash T, Hogan N (1985) The coordination of arm movements: an experimentally confirmed mathematical model. J Neurosci 5: 1688–1703
Gribble PL, Ostry DJ (1996) Origins of the power law relation between movement velocity and curvature: modeling the effects of muscle mechanics and limb dynamics. J Neurophysiol 76: 2853–2860
Grillner S (1975) Locomotion in vertebrates: central mechanisms and reflex interaction. Physiol Rev 55:247–304
Haken H, Kelso JAS, Bunz H (1985) A theoretical model of phase transition in human hand movements. Biol Cybern 51:347–356
Hollerbach JM (1981) An oscillation theory of handwriting. Biol Cybern 39:139–156
Hollerbach JM, Atkeson CG (1987) Deducing planning variables from experimental arm trajectories: pitfalls and possibilities. Biol Cybern 56:279–292
Huber PJ (1981) Robust statistics. Wiley, New York
Kay BA, Saltzman EL, Kelso JAS, Schöner G (1987) Space-time behavior of single and bimanual rhythmic movements: data and limit cycle model. J Exp Psychol Hum Percept Perform 13:178–192
Kelso JAS (1994) Elementary coordination dynamics. In: Swinnen S (ed) Interlimb coordination: neural, dynamical, and cognitive constraints. Academic Press, New York, pp 301–318
Korane KJ (1991) Sending a robot out to do a man's job. Machine Design 63:46–49
Lacquaniti F, Terzuolo C, Viviani P (1983) The law relating the kinematic and figural aspects of drawing movements. Acta Psychol 54:115–130
Lashley KS (1951) The problem of serial order in behavior. In: Jeffress LA (ed) Cerebral mechanisms in behavior, the Hixon symposium. Wiley, New York, pp 112–146
Latash ML (1993) Control of human movement. Human Kinetics Publisher, Champaign, Ill
Mertens PA (1953) Speculations on the servo control of movement. In: Malcom JL, Gray JAB, Wolstenholme GEW (eds) The spinal cord. Little Brown, Boston, Mass, pp 183–198
Morasso P (1981) Spatial control of arm movements. Exp Brain Res 42:223–227
Morasso P (1983) Three dimensional arm trajectories. Biol Cybern 48:187–194
Myers RH (1990) Classical and modern regression with applications. Pws-Kent, Boston, Mass
Pellizzer G, Massey JT, Lurito JT, Georgopoulos AP (1992) Three-dimensional drawings in isometric conditions: planar segmentation of force trajectory. Exp Brain Res 92:326–227
Press WP, Flannery BP, Teukolsky SA, Vetterling WT (1989) Numerical recipes in C – the art of scientific computing. Press Syndicate, University of Cambridge, Cambridge, Mass
Schaal S, Sternad D (1998) Programmable pattern generators. International Conference on Computational Intelligence in Neuroscience (ICCIN '98), Research Triangle Park, North Carolina
Schöner G (1990) A dynamic theory of coordination of discrete movement. Biol Cybern 63:257–270
Schöner G (1994) From interlimb dynamics to trajectory formation. In: Swinnen S, Heuer J, Massion J (eds) Interlimb coordination. Academic Press, San Diego, Calif, pp 339–368
Sherrington CS (1906) The integrative action of the nervous system. Yale University Press, New Haven, Conn
Soechting JF, Ross B (1984) Psychophysical determination of coordinate representation of human arm orientation. Neuroscience 13:595–604
Soechting JF, Terzuolo CA (1986) An algorithm for the generation of curvilinear wrist motion in an arbitrary plane in three-dimensional space. Neuroscience 19:1393–1405
Soechting JF, Terzuolo CA (1987a) Organization of arm movements in three dimensional space. Wrist motion is piecewise planar. Neuroscience 23:53–61
Soechting JF, Terzuolo CA (1987b) Organization of arm movements. Motion is segmented. Neuroscience 23:39–51
Soechting JF, Lacquaniti F, Terzuolo CA (1986) Coordination of arm movements in three-dimensional space. Sensorimotor mapping during drawing movement. Neuroscience 17:295–311
Sternad D, Amazeen EL, Turvey MT (1996) Diffusive, synaptic, and synergetic coupling: an evaluation through inphase and antiphase rhythmic movements. J Motor Behav 28:255–269
Sternad D, Saltzman EL, Turvey MT (1998) Interlimb coordination in a simple serial behavior: a task dynamic approach. Hum Movement Sci 17:393–433
Uno Y, Kawato M, Suzuki R (1989) Formation and control of optimal trajectory in human multijoint arm movement – minimum torque-change model. Biol Cybern 61:89–101
Viviani P (1986) Do units of motor action really exist? (Experimental brain research, series 15*)* Springer, Berlin Heidelberg New York, pp 828–845
Viviani P, Cenzato M (1985) Segmentation and coupling in complex movements. J Exp Psychol Hum Percept Perform 11:828–845
Viviani P, Flash T (1995) Minimum-jerk, two-thirds power law, and isochrony: converging approaches to movement planning. J Exp Psychol Hum Percept Perform 21:32–53
Viviani P, Schneider R (1991) A developmental study of the relationship between geometry and kinematics in drawing movents. J Exp Psychol Hum Percept Perform 17:198–218
Viviani P, Terzuolo C (1980) Space-time invariance in learned motor skills. In: Stelmach GE, Requin J (eds) Tutorials in motor behavior. North-Holland, Amsterdam, pp 525–533
Viviani P, Terzuolo C (1982) Trajectory determines movement dynamics. Neuroscience 7:431–437
Wada Y, Kawato M (1994) Trajectory formation of arm movement by a neural network with forward and inverse dynamics models. Systems Comp Jpn 24:37–50
Wann J, Nimmo-Smith I, Wing AM (1988) Relation between velocity and curvature in movement: equivalence and divergence between a power law and a minimum jerk model. J Exp Psychol Hum Percept Perform 14:622–637
Wood JE, Meek SG, Jacobsen SC (1989) Quantitation of human shoulder anatomy for prosthetic arm control – I. Surface modelling. J Biomech 22:273–292